Applied Surface Science 439 (2018) 689–696

Contents lists available at ScienceDirect

Applied Surface Science

journal homepage: www.elsevier.com/locate/apsusc

Full Length Article

Low-temperature amorphous boron nitride on $Si_{0.7}Ge_{0.3}(001)$, Cu, and HOPG from sequential exposures of N_2H_4 and BCl_3

Steven Wolf[a], Mary Edmonds[a], Kasra Sardashti[a], Max Clemons[a], Jun Hong Park[a], Naomi Yoshida[c], Lin Dong[c], Srinivas Nemani[c], Ellie Yieh[c], Russell Holmes[d], Daniel Alvarez[d], Andrew C. Kummel[a,b,*]

[a] *Materials Science and Engineering Program, University of California, San Diego, La Jolla, CA 92093, United States*
[b] *Department of Chemistry and Biochemistry, University of California, San Diego, La Jolla, CA 92093, United States*
[c] *Applied Materials, Sunnyvale, CA 94085, United States*
[d] *Rasirc, Inc., San Diego, CA 92126, United States*

ARTICLE INFO

Article history:
Received 13 August 2017
Revised 1 January 2018
Accepted 4 January 2018
Available online 6 January 2018

Keywords:
ALD
Boron nitride
Low temperature
Etching

ABSTRACT

Low-temperature sequential exposures of N_2H_4 and BCl_3 have been performed on $Si_{0.3}Ge_{0.7}(001)$, Cu, and HOPG surfaces at 350 °C. A novel BN ALD process has been achieved on $Si_{0.3}Ge_{0.7}(001)$ with 60 cycles of BN ALD producing a uniform, pinhole-free thin film with low contamination, as characterized with XPS and AFM. On Cu and $Si_{0.3}Ge_{0.7}(001)$, XPS spectra indicated a near stoichiometric BN film. While AFM imaging indicated the deposition on Cu yielded nanometer-scale etching, conformal deposition was observed on $Si_{0.3}Ge_{0.7}(001)$. The BN ALD also nucleated on inert HOPG via step edges. *In situ* STM imaging showed that cyclic exposures at 350 °C were able to decorate step edges with features ~2 nm tall and ~200 nm wide, indicating the propensity for BN to grow in the planar direction. The N_2H_4 and BCl_3 ALD allows for the deposition of low oxygen, low carbon films, but to avoid etching, the growth should be nucleated by N_2H_4, since exposure to BCl_3 can result in the formation of volatile Cl-containing surface species on many substrates. Therefore, the formation of a stable surface nitride prior to BCl_3 exposure is necessary to prevent formation and desorption of volatile species from the substrate.

1. Introduction

Boron nitride (BN) has gained attention due to its useful thermal and mechanical properties, chemical stability, wide bandgap, and ability to be deposited on a range of metallic and semiconducting surfaces [1–5]. BN has been utilized for applications ranging from high-temperature ceramics, protective coatings, and thin layers in semiconductor devices [6–9]. Recently, BN has been investigated for use as a low-k barrier layer on Cu, which is needed to reduce interconnect resistance-capacitance delays [10]. Amorphous BN forms shorter bonds in comparison to the more commonly used TaN and TiN barrier layers potentially making it a more effective barrier layer as device scaling continues. More prominently, though, hexagonal BN (hBN) has been extensively studied for use in 2D semiconductor devices, due to its structural similarity with graphene, chemical inertness, and lack of dangling bonds/surface traps, which make it a valuable low-k dielectric [7,11] and substrate for TMD growth.

For the deposition of nitrides, most research has either focused on using thermal NH_3, which typically requires higher growth temperatures (in excess of 400 °C), or using an activated source to lower the deposition temperature, such as plasma. However, this is accomplished at the expense of damage to the substrate. For BN, previous work has shown that BN atomic layer deposition with triethylborane and NH_3 with H_2 carrier gas occurs at 600–900 °C with a growth rate of 0.7 Å/cycle on sapphire and Si, but above this window, the process was not self-limiting [12]. George and colleagues demonstrated BN ALD with a growth rate of ~1 Å/cycle with BCl_3 and NH_3 on ZrO_2 nanoparticles at 500 K, but very large exposures in excess of 10^9 Langmuirs were required to saturate the half-cycle reactions [4]. Olander et al. demonstrated that growth with BBr_3 and NH_3 occurred at 400 °C but with a growth rate of only 0.045 nm per cycle; laser-assisted ALD was required to achieve a growth rate closer to 0.1 nm per cycle [13]. For growth of hBN on 2D materials, chemical vapor deposition (CVD) is typically employed using higher temperatures (typically in the range of 650–1000 °C) [2,14–17]. As a result, developing a low-temperature ALD process with a reasonable growth rate for smaller precursor exposures would be advantageous on a variety of surfaces.

---

* Corresponding author at: Department of Chemistry and Biochemistry, University of California, San Diego, La Jolla, CA 92093, United States.

E-mail address: akummel@ucsd.edu (A.C. Kummel).

https://doi.org/10.1016/j.apsusc.2018.01.038
0169-4332/

In this work, low-temperature plasma-less deposition of BN using sequential exposures of anhydrous hydrazine (N_2H_4) and boron trichloride (BCl_3) was performed on various substrates. A SiGe substrate was chosen since 1–2 monolayers of BN could act as a barrier for transition metal dichalcogenides (TMDs) grown on Si wafers or high mobility SiGe films on Si commercial wafers. TMDs deposited on Si have been shown to improve device performance [18,19]. Cu was chosen since ultrathin diffusion barriers are needed [10,20,21], and HOPG was chosen as a model of graphene for which 1–2 monolayer dielectrics are required [7,22]. In addition, the diversity of surface reactivity enables a fundamental understanding of low-temperature BN ALD using N_2H_4 and BCl_3. By using anhydrous N_2H_4 as the reactive nitrogen source, the reaction with BCl_3 can proceed at a lower temperature than NH_3, while preventing oxygen incorporation into BN films, as previously demonstrated with SiN_x films [23]. Chloride-containing precursors, such as BCl_3, $TiCl_4$, Si_2Cl_6, are ideal for nitride ALD because of their favorable thermochemistry that induces an HCl(g) desorption product, ultimately leaving minimal unreacted Cl ligands in the deposited film. The contamination and excess Cl has been correlated with unfavorable properties in TiN films [24,25]; therefore, maintaining a clean, nearly stoichiometric film is desirable. Furthermore, chlorine precursors can induce etching via formation and desorption of volatile species (i.e. $SiCl_4$, Cu_3Cl_3), thereby roughening the substrate. In the present report, a self-limiting and saturating BN ALD occurred on $Si_{0.7}Ge_{0.3}(001)$ with 60 cycles of BN ALD, which produced a uniform, nearly contamination-free film. The same precursors were sequentially exposed to Cu and HOPG substrates with the goal of achieving an ALD process, but the RMS surface roughness increase on Cu was consistent with precursor etching induced by the formation and desorption of volatile Cu species. On HOPG, nucleation was achieved at step edges with N_2H_4, and subsequent cycles of N_2H_4 and BCl_3 were performed at 350 °C, leading to anisotropic growth in the planar direction. Ultimately, low oxygen, low carbon BN was deposited, but to avoid any etching by the precursors, the growth should be nucleated by N_2H_4 to form a stable surface nitride that can protect the surface from any etching caused by BCl_3.

2. Experimental

This study utilized 12 nm thick p-type $Si_{0.7}Ge_{0.3}(001)$ that was epitaxially grown on a p-type Si(001) substrate (Applied Materials), 50 nm sputtered Cu on SiO_2/Si (Applied Materials), and HOPG purchased from SPI Supplies. $Si_{0.7}Ge_{0.3}(001)$ samples underwent an *ex situ* wet clean involving a 10 min sonication in acetone, a 10 min sonication in isopropyl alcohol, a 5 min sonication in DI water, followed by a 2 min etch in 2% HF/H_2O. The samples were wetted with toluene to prevent surface oxidation before being loaded into the vacuum chamber with minimal air exposure. Once loaded into the UHV chamber (Fig. 1), the samples were heated to 330 °C for 15 min and subsequently dosed with 1×10^{-6} Torr of atomic hydrogen for 30 min (1800 Langmuirs) to remove surface carbon contamination. Atomic H was generated by flowing H_2 through a thermal gas cracker (Applied Research) operated at 65 W. The

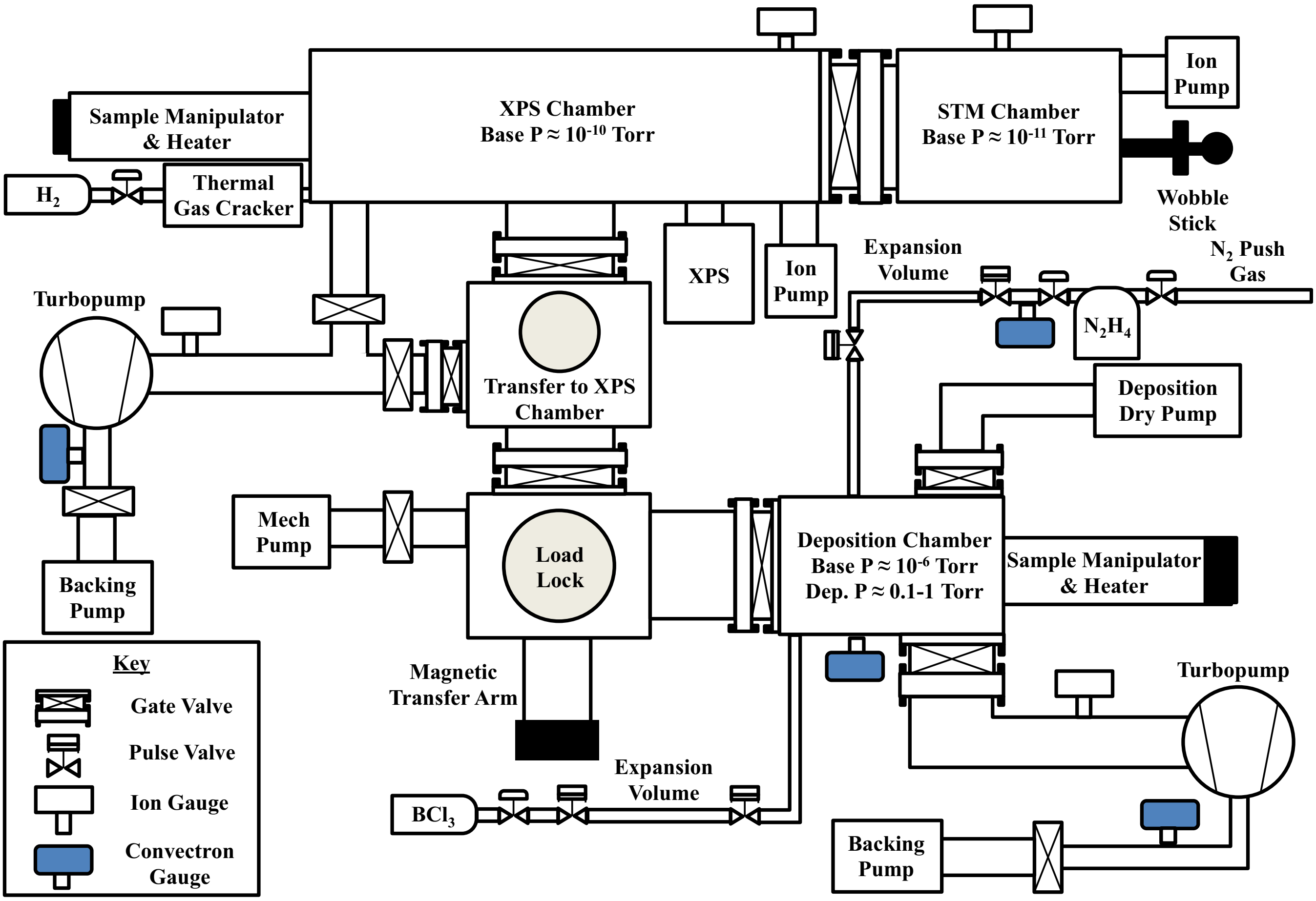

Fig. 1. Chamber schematic. The system used for BN deposition was comprised of a load lock chamber, deposition chamber, XPS chamber, and STM chamber. After BN deposition, samples were transferred in vacuum without ambient exposure to perform *in situ* XPS and STM analysis.

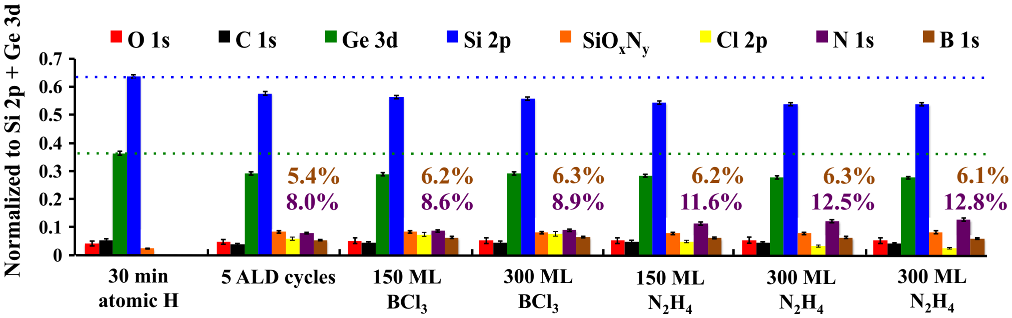

Fig. 2. Saturation study of BN growth on $Si_{0.7}Ge_{0.3}$(001). Atomic H clean was performed at 330 °C, and 5 ALD cycles of 150 ML N_2H_4 and 150 ML BCl_3 exposures were performed at 350 °C. The percentage of nitrogen (purple) and boron (brown) are explicitly listed for each experiment. Each exposure is in addition to the previous surface treatment. (For interpretation of the references to colour in this figure legend, the reader is referred to the web version of this article.)

exposures were calculated for maximum cracking efficiency, but the actual efficiency was likely 30–50%. Cu samples were annealed in UHV at 350 °C to drive off surface contamination, as well as dosed with atomic H to further remove contamination. HOPG was exfoliated with tape prior to being loaded into vacuum and subsequently annealed at 400 °C for 30 minutes to remove physisorbed hydrocarbons from the surface.

Precursor exposures were performed in a deposition chamber that was separated from the UHV chamber by a gate valve (Fig. 1). The deposition chamber with attached precursor dosing lines was pumped by a turbomolecular pump that yielded a base pressure of 2×10^{-6} Torr. The entire chamber, precursor dosing lines, and connecting line to the dry pump were all continuously heated to 80–100 °C to ensure both precursors would not condense to the chamber walls and react to form any solid powder byproduct. In addition, the N_2H_4 vessel was pressurized to atmospheric pressure with ultrahigh purity N_2 to act as a carrier gas. Note that reported N_2H_4/N_2 exposures below are reported as N_2H_4 exposures, and the actual N_2H_4 exposures are lower due to the dilution in N_2; from the vapor pressure of N_2H_4, the estimated fraction of N_2H_4 is approximately 1.5%. Samples were preheated in the UHV chamber before being transferred to the deposition chamber where they were radiatively heated by a PBN heater. After exposure to anhydrous N_2H_4 (Rasirc) and BCl_3 (Praxair), samples were transferred back to the UHV chamber where X-ray photoelectron spectroscopy (XPS) could be performed without breaking vacuum. An *in situ* monochromatic XPS system (Al kα hν = 1486.7 eV) was used to collect spectra at an angle of 30° with respect to the surface parallel, a pass energy of 50 eV, and a line width of 0.1 eV. XPS analysis was conducted with CASA XPS v.2.3 and included Shirley background subtractions. Raw peak areas were corrected by Schofield photoionization cross sectional relative sensitivity factors. For Cu XPS spectra, the data was additionally corrected by the inelastic mean free paths due to the binding energy of Cu 2p being much larger than the other analyzed peaks. Along with *in situ* XPS, *in situ* scanning tunneling microscopy (STM) utilized constant current mode with a tip bias of +2 V and current set point of 20 pA. Lastly, atomic force microscopy (AFM) was employed to image the surfaces.

3. Results

3.1. A. $Si_{0.7}Ge_{0.3}$(001)

To determine the half-cycle dose sizes, as well as check for saturation dosing on $Si_{0.7}Ge_{0.3}$(001), XPS was used to monitor successive exposures. Fig. 2(a) shows the XPS corrected peak areas normalized to the sum of Si 2p and Ge 3d for the $Si_{0.7}Ge_{0.3}$(001) surface. The surface was cleaned with 1800L atomic H at 330 °C, followed by 5 cycles of 150 ML N_2H_4 and 150 ML BCl_3 to establish baseline N 1s and B 1s signals; the 5 ALD cycles terminated with a BCl_3 pulse. An additional 150 ML and 300 ML exposure of BCl_3 shows essentially no change in the B 1s signal, indicating saturation of the BCl_3 half-cycle. Similarly, 150 ML exposures of N_2H_4 (1/2 cycle ALD) followed by additional 300 ML exposures indicated the surface was nearly saturated after a total of 450 ML of N_2H_4 from the negligible increase in the N 1s signal during the last 300 ML N_2H_4 exposure; this confirmed the self-limiting ALD of BN on $Si_{0.7}Ge_{0.3}$(001). It should be noted that the amount of Cl dropped from ~8% to ~2% after N_2H_4 dosing, but was unable to be fully removed at a relatively low reaction temperature of 350 °C by large N_2H_4 exposures. At this sample temperature, saturated amounts of half-cycle exposures were crucial for maximizing ligand exchange on the surface to leave minimal Cl residue in the film.

After checking for saturation, thicker films were deposited using saturation pulses (300 ML BCl_3 + 450 ML N_2H_4 per ALD cycle). Fig. 3(a) shows the XPS after 5, 30, and 60 cycles of BN on $Si_{0.7}Ge_{0.3}$(001) normalized to Si 2p + Ge 3d. Additionally, a final atomic H clean at 285 °C for 20 min was performed to remove any remaining surface Cl. Fig. 3(b) shows the raw Si 2p, B 1s, and N 1s peaks for the normalized data. The Si 2p peak attenuates, while the B 1s peak at ~190.5 eV and the N 1s peak at ~398 eV grow as a function of the number of cycles, in good agreement with previously reported binding energies [26,27]. After 5 cycles, a broader N 1s peak was observed, which is indicative of the presence of an interfacial nitride between the boron nitride and $Si_{0.7}Ge_{0.3}$(001) surface. Note that the initial dosing by N_2H_4 formed this surface nitride, as evidenced by the higher binding energy component in the Si 2p region at ~101.7 eV, corresponding to an interfacial SiN_x. This interfacial SiN_x layer caused the deposited film to appear nitrogen-rich (B:N ratio = 0.45) after 5 ALD cycles of $BCl_3 + N_2H_4$ due to the Si—N bond formation detected in XPS. After 60 ALD cycles, the substrate Si 2p and Ge 3d peaks as well as interfacial SiN_x component were nearly fully attenuated; therefore; the ratio of B:N shifted to 1.13. By using saturated ALD half cycles, the amount of residual chlorine in the film was reduced to 2.5% after atomic H exposure for the 60 ALD cycles at 350 °C to remove surface Cl. This BN film was estimated to be ~5 nm thick by accounting for the Si 2p signal attenuation and electron escape depth. Due to the demonstration of saturating half-cycles in Fig. 2, a fairly constant growth rate of ~0.08 nm/cycle was estimated. As a result, nearly stoichiometric amorphous BN was formed with low levels of oxygen, carbon, and chlorine incorporation (<5%) on $Si_{0.7}Ge_{0.3}$(001).

To determine film conformality, AFM was conducted on the HF-cleaned and BN deposited surfaces (Fig. 4). The HF-cleaned

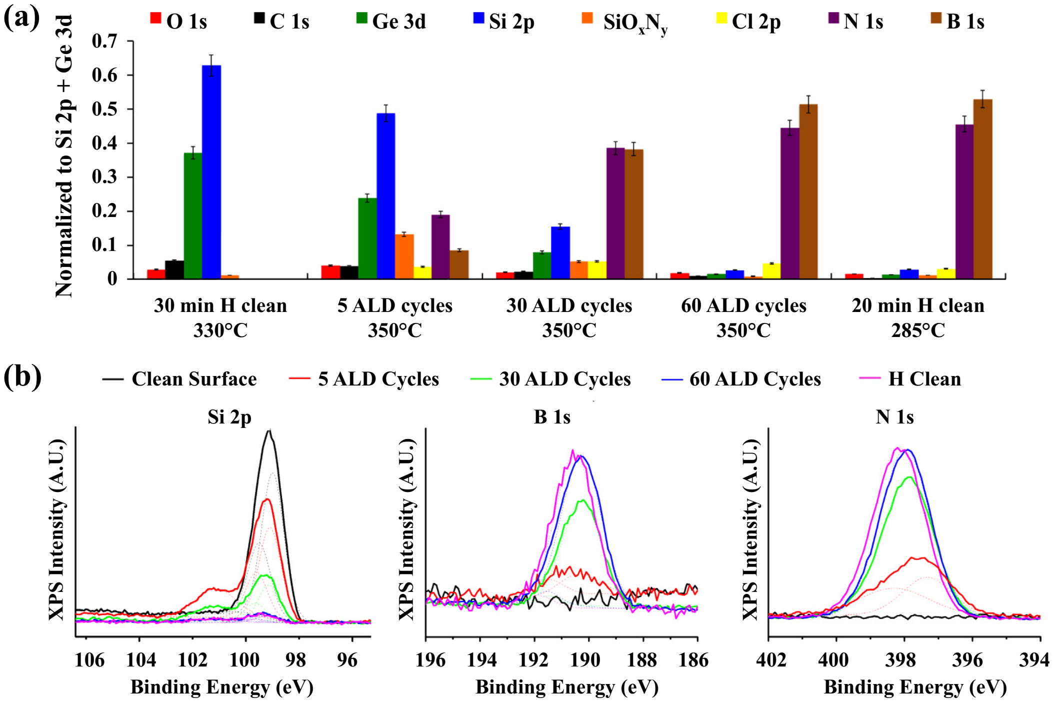

Fig. 3. XPS of BN Growth on $Si_{0.7}Ge_{0.3}(001)$. (a) XPS corrected peak areas normalized to Si 2p + Ge 3d for clean surface, 5 cycles, 30 cycles, and after 60 cycles BN. A final H clean was performed to remove surface Cl. (b) XPS Si 2p, B 1s, and N 1s raw peak areas for the clean surface after 5 cycles, 30 cycles, and 60 cycles. Note the formation of a higher binding energy SiN_x component after 5 ALD cycles.

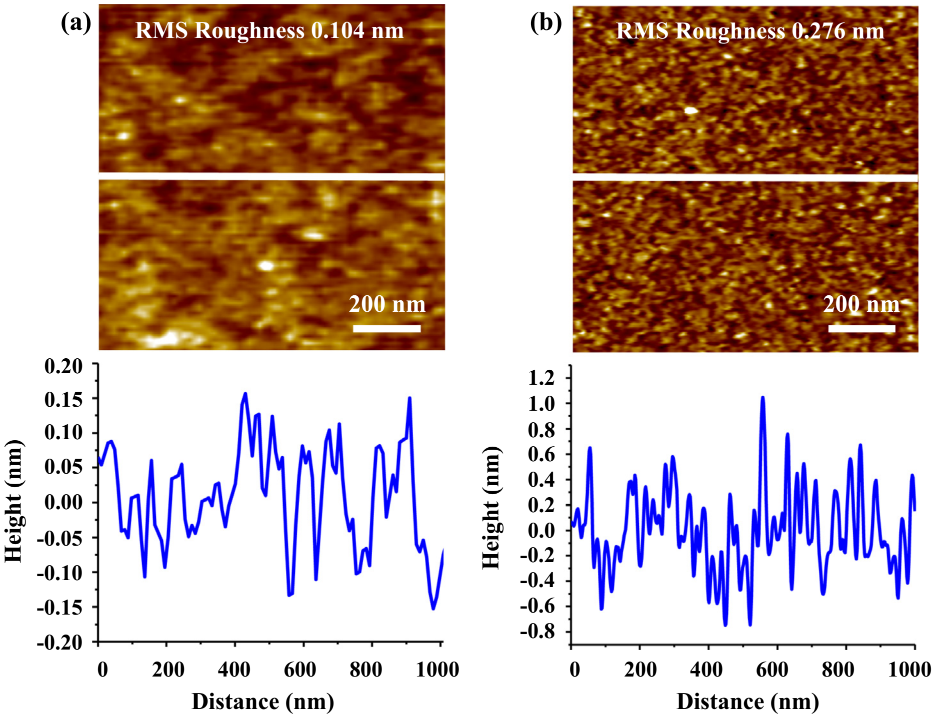

Fig. 4. AFM of BN growth on $Si_{0.7}Ge_{0.3}(001)$. 1 μm × 1 μm AFM images of (a) HF treated $Si_{0.7}Ge_{0.3}(001)$ and (b) 60 cycles BN ALD on $Si_{0.7}Ge_{0.3}(001)$.

surface (Fig. 4(a)) was extremely flat and had a corresponding root mean square (RMS) surface roughness of 0.104 nm for a 1 μm × 1 μm area. The RMS roughness after 60 cycles of BN deposition was still only 0.276 nm; this sub-nanometer roughness and lack of evidence of pinholes was consistent with the ALD BN deposition on $Si_{0.7}Ge_{0.3}(001)$ being conformal. To further investigate the quality of the 60 cycles BN film, metal-oxidesemiconductor insulator-capacitors (MOSCAPs) were fabricated by depositing 50 nm of 150 μm Ni dots on the BN layer (see supplementary information Fig. S1). Corresponding capacitance-voltage and current-voltage measurements indicated that the film was sufficiently insulating and pinhole free by achieving a capacitance

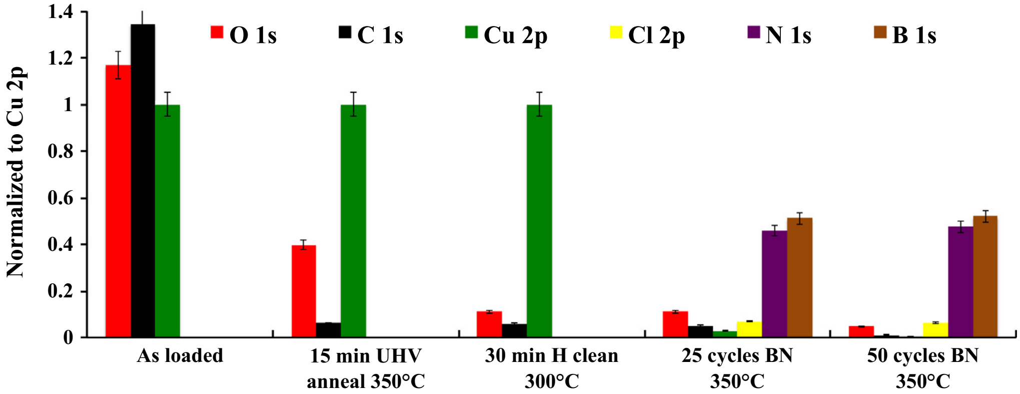

Fig. 5. BN Growth on Cu. XPS of as loaded, UHV annealed, atomic H cleaned and after 25 and 50 cyclic exposures to N_2H_4 and BCl_3. After 50 cycles, 4.8% oxygen, 6.4% chlorine, and <1% carbon were present in the film.

and measuring a leakage of $2.69 * 10^{-4}$ A/cm^2 at a gate bias of −2 V after a forming gas anneal. For integration of TMDs on commercial 300 mm Si wafers, or high-hole mobility SiGe films on Si wafers, an insulating ultrathin diffusion barrier is needed [18,28]. This pinhole-free BN layer on $Si_{0.7}Ge_{0.3}(001)$ shows the ease of formation of insulating nanoscale BN on commercial wafers.

3.2. B. Cu

As a comparison to the $Si_{0.3}Ge_{0.7}(001)$ surface, sequential exposures of N_2H_4 and BCl_3 were performed on Cu on SiO_2/Si. Fig. 5 shows the XPS spectra corrected with Schofield values and inelastic mean free paths normalized to Cu 2p. XPS was collected for the as loaded, UHV annealed, and atomic H cleaned surface, and after BN cycles at 350 °C using the saturation conditions determined by the ALD on $Si_{0.3}Ge_{0.7}(001)$. From XPS characterization, the final film after 50 ALD cycles had less than 5% oxygen incorporation, negligible carbon, and only 6% Cl. Note, in contrast to the $Si_{0.7}Ge_{0.3}(001)$ surface, no surface nitride was present on the Cu 2p peak. Although the substrate Si signal was absent after the 50 ALD cycles, consistent with the Cu layer being intact, AFM studies showed an increase in surface roughness after ALD consistent with slight etching of Cu. The slightly higher amount of Cl for ALD on Cu vs. $Si_{0.7}Ge_{0.3}(001)$ can be attributed to using non-optimized dosing conditions for the Cu study.

To study the surface topography, AFM images were taken of the as loaded sample (Fig. 6(a)) after the atomic H clean (b) and after 50 cycles (c). Note the AFM image taken after the atomic H clean required exposing the sample to air and likely surface oxidation. After atomic H cleaning, there was a noticeable change in the surface topology, consistent with Cu grain growth; this phenomena is attributed to a driving force to reduce Cu grain boundary energy [29]. Small ∼2–4 nm deep holes were also present, attributed to inhomogeneous atomic H etching [30]. The RMS roughness of the as loaded surface was 1.259 nm; after the H clean and air exposure, it was 2.886 nm, and after the 50 cycles of BN, it was 7.519 nm. The increase in the RMS roughness was correlated with an increase in Cu grain coarsening, but etching cannot be excluded.

3.3. C. HOPG

BN deposition was studied on HOPG and characterized with in-situ XPS and STM. Fig. 7(a) shows a 50 nm × 50 nm STM image of clean HOPG UHV annealed at 400 °C for 1 hour. To check for reactivity on HOPG, large initial exposures of (b) BCl_3 and (c) N_2H_4 were performed. To ensure sufficient exposure, 500 ML BCl_3 was exposed to the HOPG surface; however, virtually no B 1s or Cl 2p counts were detected with XPS, and the corresponding STM image showed only minor bright sites that might have indicated reactivity at defects. Similarly, after several pulses corresponding to 15 ML of N_2H_4 exposure to the clean HOPG surface, the N 1s XPS signal could not be detected; however, in STM, clear 1.7 ± 0.3 nm tall features were present on the surface at the step edges. This is consistent with nucleation by N_2H_4. Since an XPS saturation study could not be executed due to insignificant changes in coverage during half cycle exposures, additional ALD cycles were dosed and characterized with XPS. To further study the growth of BN on these features, 30 cycles of 5 ML BCl_3 + 2 ML N_2H_4 (corresponding to 1 second pulses) were performed. The corresponding STM images presented in Fig. 8. Show the ALD induced features have a maximum height of ∼2.2 nm and a width of ∼100–200 nm. In XPS, the films showed ∼8% B and 7% N with Cl and O both comprising less than 1% of the film concentration normalized to the area of C 1s after 30 cycles (Fig. 9). It should be noted that half cycle reactions did not appear to saturate in a traditional ALD sense as shown by STM imaging; when half-cycle exposures of N_2H_4 and BCl_3 became too large (>10 ML), evidence of substrate etching near the decorated step edges was observed (Fig. S2). Since only 1–2 monolayer of BN would be needed in a practical device, this may not be significant in some applications.

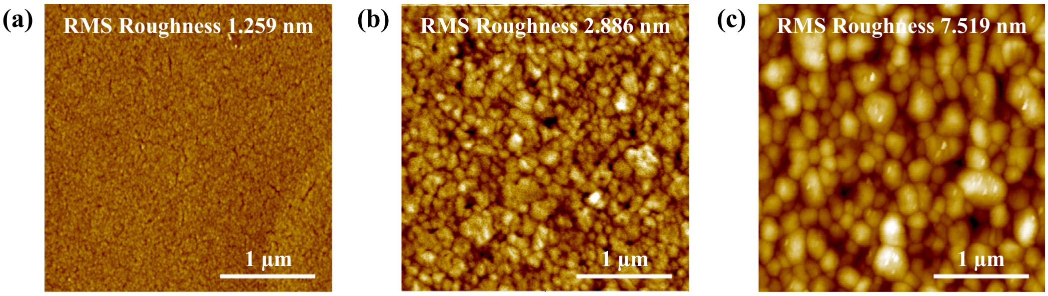

Fig. 6. AFM of Cu samples. 3 μm × 3 μm AFM images of (a) as loaded Cu, (b) after H clean and air exposure, and (c) after 50 cycles of sequential exposures of N_2H_4 and BCl_3.

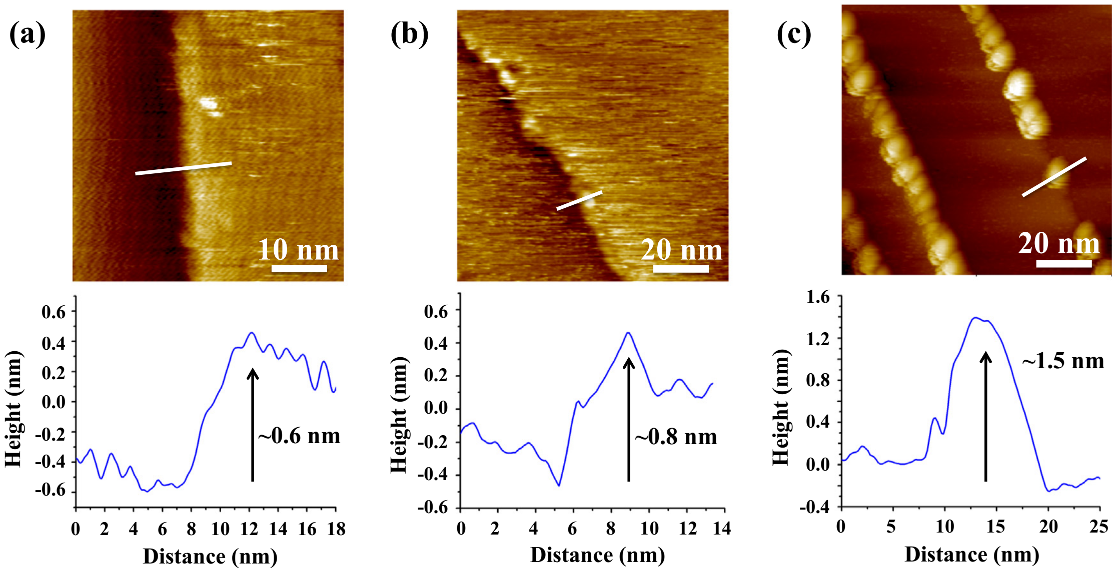

Fig. 7. *In situ* STM images of HOPG before and after 1 cycle of $BCl_3 + N_2H_4$. STM images of (a) tape-cleaned HOPG annealed at 400 °C for 1 h, (b) after 500 ML BCl_3 exposure at 350 °C, and (c) after 15 ML N_2H_4 exposure at 350 °C.

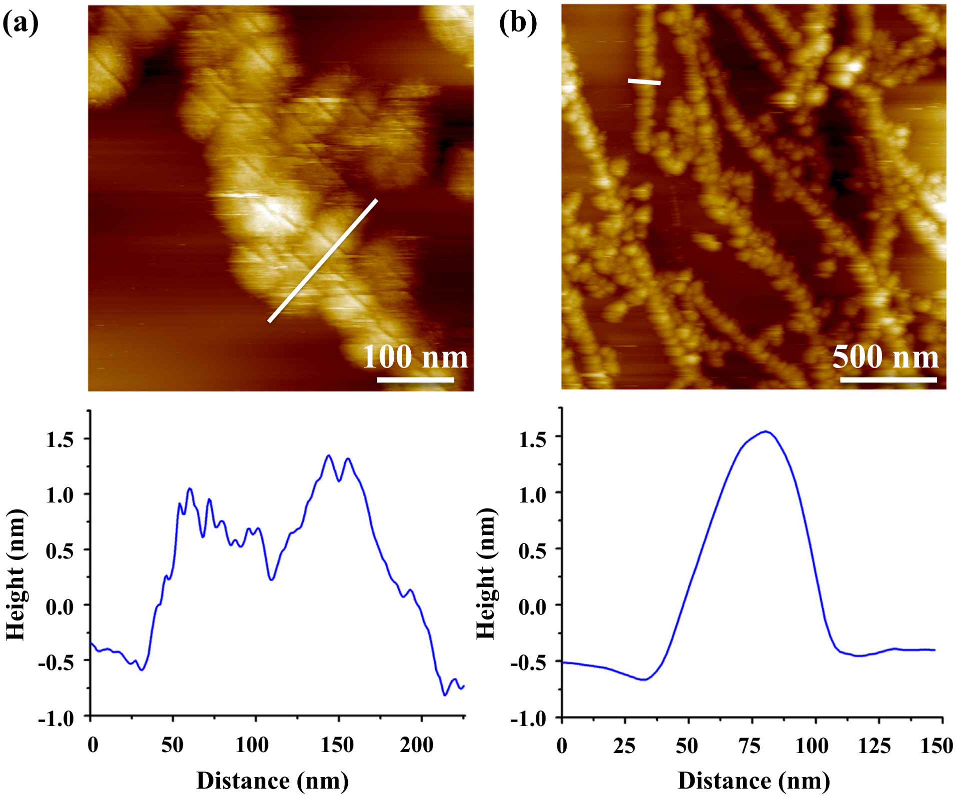

Fig. 8. *In Situ* STM images of HOPG before and after 30 cycles of $BCl_3 + N_2H_4$. (a) 500 nm × 500 nm and (b) 2 μm × 2 μm STM images and respective line traces of 30 cycles of 5 ML BCl_3 + 2 ML N_2H_4.

4. Discussion and conclusion

To understand the mechanism of ALD on $Si_{0.3}Ge_{0.7}(001)$, in comparison to the etching witnessed on Cu, it is first necessary to understand the surface chemistry. On $Si_{0.3}Ge_{0.7}(001)$, N_2H_4 was observed to nitridate the surface, forming Si—NH_x bonds, as previously reported [23]. By forming a surface with Si—NH_x, subsequent half-cycle dosing with BCl_3 is well suited to form Si—N—BCl_x with an HCl(g) desorption product. This surface nitridation prevents BCl_3 and perhaps any Cl byproducts from reaching the surface and forming Si—Cl_x species, such as volatile $SiCl_4$. On Cu, the driving force to form Cu—NH_x bonds is low since the standard heat of formation of Cu_3N is endothermic [31]; hence, no shifted Cu—N component is seen in the Cu 2p XPS spectrum. Due to this poor

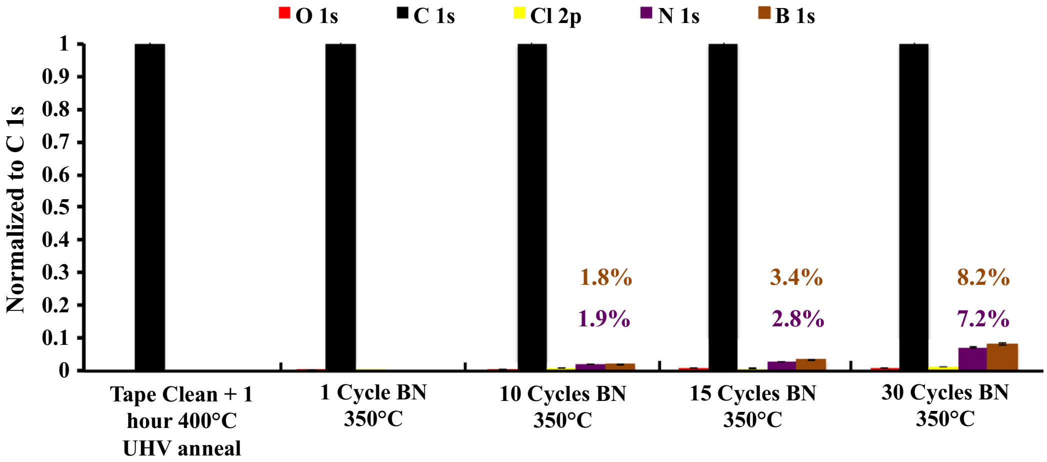

Fig. 9. XPS of BN growth on HOPG. (a) XPS corrected peak areas normalized to C 1s for the clean HOPG surface followed by BN cycles at 350 °C. Only C 1s is detectable through the first cycle of BN. Additional cycles leads to <1% concentrations of O and Cl on the surface.

reactivity, and hence poor passivation, this allows BCl_3 and potential Cl_2 gas to find Cu sites and induce formation of volatile Cu—Cl species, such as Cu_3Cl_3. This tendency for Cu—Cl formation, coupled with non-optimized dosing on Cu, can help explain the larger amount of Cl residue seen in the BN film on Cu in comparison to residues seen in films grown on $Si_{0.3}Ge_{0.7}(001)$ and HOPG surfaces.

After cyclic exposures, the BN grew anisotropically out from the step edges corresponding to 5.0 ± 1.7 nm/cycle in the planar direction compared to only 0.05 ± 0.01 nm/cycle in the vertical direction based on the average final feature size after 30 cycles of deposition. Due to the etching that was witnessed near the decorated step edges from non-saturating exposures greater than 10 ML, the quantification of growth rate was challenging, and thus the accuracy of these numbers is limited. However, these values support the hypothesis that nitrided HOPG step edges were required to catalyze the reaction leading to the higher growth rate in the planar dimension. This propensity to grow in the planar direction can further support the pinhole-free film seen on $Si_{0.3}Ge_{0.7}(001)$ and the corresponding electrical data (Fig. S1).

A novel BN ALD process at 350 °C has been accomplished on the $Si_{0.3}Ge_{0.7}(001)$ surface using N_2H_4 and BCl_3 with the resulting BN thin film being uniform and pin-hole free. Nearly stoichiometric amorphous BN with low oxygen, carbon, and chlorine incorporation resulted. The sufficiently insulating pinhole-free amorphous BN film could be used for the integration of TMDs on commercial wafers, in which an ultrathin diffusion barrier is needed. On HOPG, the N_2H_4 was reactive to the step edges, and subsequent cycles after the initial decoration displayed the tendency for BN films to grow anisotropically in the planar direction. Therefore, in general, for substrates that can react with N_2H_4 and form a nitride protection layer, amorphous BN should be grown without etching of the substrate when using BCl_3. The resulting films will be oxygen and carbon free, as well as conformal.

Acknowledgments

This work was performed in part at the San Diego Nanotechnology Infrastructure (SDNI) of UCSD, a member of the National Nanotechnology Coordinated Infrastructure, which is supported by the National Science Foundation (Grant ECCS-1542148) and by SWAN, a funded center of NRI, a Semiconductor Research Corporation (SRC) program sponsored by NERC and NIST. Additionally, the authors would also like to thank Rasirc, Inc and Applied Materials, Inc, for further support, as well as Michael Breeden for the chamber schematic.

Appendix A. Supplementary material

Supplementary data associated with this article can be found, in the online version, at https://doi.org/10.1016/j.apsusc.2018.01.038.

References

[1] H.O. Pierson, Handbook of Refractory Carbides & Nitrides: Properties, Characteristics, Processing and Apps, William Andrew, 1996.
[2] K.K. Kim et al., Synthesis of monolayer hexagonal boron nitride on Cu foil using chemical vapor deposition, Nano Lett. 12 (1) (2011) 161–166.
[3] R.Y. Tay et al., Growth of large single-crystalline two-dimensional boron nitride hexagons on electropolished copper, Nano Lett. 14 (2) (2014) 839–846.
[4] J. Ferguson, A. Weimer, S. George, Atomic layer deposition of boron nitride using sequential exposures of BCl_3 and NH_3, Thin Solid Films 413 (1) (2002) 16–25.
[5] A. Haider et al., Low-temperature deposition of hexagonal boron nitride via sequential injection of triethylboron and N_2/H_2 plasma, J. Am. Ceram. Soc. 97 (12) (2014) 4052–4059.
[6] A. Lipp, K.A. Schwetz, K. Hunold, Hexagonal boron nitride: fabrication, properties and applications, J. Eur. Ceram. Soc. 5 (1) (1989) 3–9.
[7] C.R. Dean et al., Boron nitride substrates for high-quality graphene electronics, Nat. Nanotechnol. 5 (10) (2010) 722–726.
[8] A. Bath et al., Plasma enhanced chemical vapor deposition and characterization of boron nitride gate insulators on InP, J. Appl. Phys. 70 (8) (1991) 4366–4370.
[9] S. Nguyen et al., Plasma-assisted chemical vapor deposition and characterization of boron nitride films, J. Electrochem. Soc. 141 (6) (1994) 1633–1638.
[10] S. King et al., X-ray photoelectron spectroscopy investigation of the Schottky barrier at a-BN: H/Cu interfaces, Electrochem. Solid-State Lett. 14 (12) (2011) H478–H479.
[11] L. Britnell et al., Field-effect tunneling transistor based on vertical graphene heterostructures, Science 335 (6071) (2012) 947–950.
[12] M. Snure et al., Optical characterization of nanocrystalline boron nitride thin films grown by atomic layer deposition, Thin Solid Films 571 (1) (2014) 51–55.
[13] J. Olander et al., Laser-assisted atomic layer deposition of boron nitride thin films, Chem. Vap. Deposition 11 (6–7) (2005) 330–337.
[14] L. Ci et al., Atomic layers of hybridized boron nitride and graphene domains, Nat. Mater. 9 (5) (2010) 430–435.
[15] L. Song et al., Large scale growth and characterization of atomic hexagonal boron nitride layers, Nano Lett. 10 (8) (2010) 3209–3215.
[16] Z. Liu et al., Direct growth of graphene/hexagonal boron nitride stacked layers, Nano Lett. 11 (5) (2011) 2032–2037.
[17] A. Hemmi et al., High quality single atomic layer deposition of hexagonal boron nitride on single crystalline Rh (111) four-inch wafers, Rev. Sci. Instrum. 85 (3) (2014) 035101.
[18] M.-C. Chen et al., Hybrid Si/TMD 2D electronic double channels fabricated using solid CVD few-layer-MoS2 stacking for V th matching and CMOS-compatible 3DFETs, Electron Devices Meeting (IEDM), 2014 IEEE International, IEEE, 2014.
[19] L. Wang et al., MoS2/Si heterojunction with vertically standing layered structure for ultrafast, high-detectivity, self-driven visible-near infrared photodetectors, Adv. Funct. Mater. 25 (19) (2015) 2910–2919.
[20] A. Kaloyeros, E. Eisenbraun, Ultrathin diffusion barriers/liners for gigascale copper metallization, Annu. Rev. Mater. Sci. 30 (1) (2000) 363–385.
[21] F. Braud et al., Ultra thin diffusion barriers for Cu interconnections at the gigabit generation and beyond, Microelectron. Eng. 33 (1–4) (1997) 293–300.

[22] M.C. Lemme et al., A graphene field-effect device, IEEE Electron Device Lett. 28 (4) (2007) 282–284.

[23] M. Edmonds et al., Low temperature thermal ALD of a SiNx interfacial diffusion barrier and interface passivation layer on SixGe1− x(001) and SixGe1− x(110), J. Chem. Phys. 146 (5) (2017) 052820.

[24] M. Burke et al., Low sheet resistance titanium nitride films by low-temperature plasma-enhanced atomic layer deposition using design of experiments methodology, J. Vacuum Sci. Technol. A: Vacuum Surf. Films 32 (3) (2014) 031506.

[25] J. Musschoot et al., Atomic layer deposition of titanium nitride from TDMAT precursor, Microelectron. Eng. 86 (1) (2009) 72–77.

[26] D.N. Hendrickson, J.M. Hollander, W.L. Jolly, Core-electron binding energies for compounds of boron, carbon, and chromium, Inorg. Chem. 9 (3) (1970) 612–615.

[27] R. Trehan, Y. Lifshitz, J. Rabalais, Auger and x-ray electron spectroscopy studies of h BN, c BN, and N+ 2 ion irradiation of boron and boron nitride, J. Vacuum Sci. Technol. A: Vacuum Surf. Films 8 (6) (1990) 4026–4032.

[28] Y. Liu et al., Growth and humidity-dependent electrical properties of bulk-like MoS 2 thin films on Si, RSC Adv. 5 (91) (2015) 74329–74335.

[29] S. Du, Y. Li, Effect of annealing on microstructure and mechanical properties of magnetron sputtered Cu thin films, Adv. Mater. Sci. Eng. 2015 (2015).

[30] F. Wu, G. Levitin, D.W. Hess, Low-temperature etching of Cu by hydrogen-based plasmas, ACS Appl. Mater. Interfaces 2 (8) (2010) 2175–2179.

[31] W.F. Gale, T.C. Totemeier, Smithells Metals Reference Book, Butterworth-Heinemann, 2003.